Water Temperature and Energy Balance of Floating Photovoltaic Construction Water Area—Field Study and Modeling

Zhao Liu[1,2], Chao Ma[1,2,4*], Yilin Yang[3], Xinyang Li[1,2], Haixing Gou[1,2], Andrew M. Folkard[5]

[1]State Key Laboratory of Hydraulic Engineering Intelligent Construction and Operation, Tianjin University, Tianjin 300072, China.

[2]School of Civil Engineering, Tianjin University, Tianjin 300350, China.

[3]Tianjin Key Laboratory of Water Resources and Environment, Tianjin Normal University, Tianjin 300387, China.

[4]School of Civil and Traffic Engineering, Qinghai Minzu University, Qinghai 810007, China.

[5]Lancaster Environment Centre, Library Avenue, Lancaster University, Lancaster, LA1 4YQ, United Kingdom.

Corresponding author: Chao Ma (e-mail: mac_tju@tju.edu.cn)

Abstract

Floating photovoltaics (FPV) are emerging renewable energy technology. Although they have received extensive attention in recent years, the understanding of their environmental impacts is limited. To address this knowledge gap, this paper reports field work and numerical modeling focusing on water temperature as the key parameter. The results show that FPVs have a cooling effect on their host waterbody during the daytime and a thermal insulation effect at night. The diel oscillation of water temperature below the FPV panels lags behind that in open waters by a timescale on the order of two hours. Water stability and stratification are weakened during the daytime but enhanced at night. Wind speed below the FPV panels is reduced by 70%. The air temperature below the FPV panels increases during the daytime (+2.01°C) and decreases at night (-1.27°C) on average, while the relative humidity

changes in reverse (-3.72%, +14.43%). The change of water temperature is related to local climate conditions. The impact of FPV on water temperature and water stability would be more significant if the FPV systems were in tropical, humid and low wind-speed areas. The numerical model could capture the energy balance characteristics with a correlation coefficient of 0.82 between the simulated and actual data. The shortwave radiation below the FPV panels is significantly reduced and the longwave radiation emitted by FPV panels becomes one of the heat sources during the daytime. The latent heat flux is significantly reduced, while the changes in sensible heat flux are unnoticeable. The energy balance and water temperature below the FPV panels are primarily controlled by the significant decrease in thermal income from shortwave radiation and thermal expenditure from longwave radiation and latent heat flux. The measured data and simulation results serve as a foundation for evaluating the impact of FPV systems on water temperature, energy budget, and aquatic environment, which would also provide a more comprehensive understanding of FPV systems.

Highlights:

- The field study of FPV construction water area is completed and the field data is collected.
- The numerical model is established to characterize the water energy balance.
- The influence of FPV on water temperature and local microclimatic conditions is analyzed.
- The relationship between meteorological parameters and the change in water temperature is expounded.
- The composition and variation of heat fluxes under the influence of FPV are revealed.

Keywords: floating photovoltaic, water temperature, energy balance, field study, modeling, microclimate

1 Introduction

As one of the most promising renewable energy sources, solar energy has made a significant contribution to the global green energy revolution and the achievement of decarbonization goals (Solomin et al., 2021). Photovoltaic power generation is an easy and effective way to capture solar energy (Hosenuzzaman et al., 2015). However, in the context of the rapid growth of energy-water-food demand, for many countries with scarce land and dense populations, the large-scale deployment of photovoltaic power plants is often hindered by a shortage of agricultural and residential land (Zhou et al., 2020). The rapid rise and development of floating photovoltaics (FPV) in recent years has provided a new solution to this problem (Spencer et al., 2019). FPV refers to power generation systems built on the surface of lentic waters such as lakes, reservoirs, ponds, and coal mining subsidence areas (Sahu et al., 2016). This new form of power generation has been developed primarily in China, Japan and South Korea, but is also present in several other countries or regions (Trapani and Redón Santafé, 2015). As of August 2020, the installed capacity of FPV built in the world was calculated to be 2.6 GW (Manoj Kumar et al., 2022). An ever-increasing number of theoretical and empirical studies have shown that FPV has significant advantages over conventional land-based photovoltaics. The growth of FPV has made an important contribution to ensuring energy supply security, reducing carbon emissions, and creating additional water and food benefits (Oliveira-Pinto and Stokkermans, 2020; McKuin et al., 2021; Gadzanku et al., 2021).

An important issue to address in the context of rapid development of FPV is the potential, especially for large-scale, high-coverage projects, for significant impacts on the aquatic environment (Hooper et al., 2021; Gorjian et al., 2021). However, this issue has received little research attention to date. The shading of FPV reduces the amount of solar radiation reaching the water surface and the

wind shear stress as the water surface, which together impact on water temperature (Exley et al., 2021). Water temperature serves as the foundation parameter for exploring the physical properties, chemical processes, and biodiversity of water bodies (Yang et al., 2019). Therefore, revealing the impact of FPV on the water energy balance through water temperature is crucial to comprehending its impact on the aquatic environment. Some researchers have explored the effects of different cover materials, geometric shapes, and colors on water energy balance (Assouline and Narkis, 2021; Rezazadeh et al., 2020; Mady et al., 2021; Shalaby et al., 2021a; Shalaby et al., 2021b; Lehmann et al., 2019). There also have been several studies of FPV's effects on water temperature. Exley et al. (2021) used a one-dimensional process-based MyLake v1.2 model to simulate the effects of FPV-induced changes in wind speed and solar radiation on lake thermal structure. They found that, as the percentage of the water surface covered by FPV increased, wind speed and solar irradiation decreased, and water temperature reduced non-linearly. Ilgen and Schindler et al. (2023) found that the cooling effect of FPV on water temperature was mainly reflected in the upper water body during high-temperature periods. The effect of FPV on water temperature was cooling during the daytime and heat retaining at night. The heat storage in open waters was higher than that below the FPV panels during the daytime and lower at night. Water quality monitoring by Bax et al. (2023) found that FPV reduced the availability of light beneath them by 73% to 100%, but that the impact of FPV on water temperature was limited. Ji et al. (2022) established the Ce-qual-W2 model, which predicted that FPV could reduce water temperature, water age, and relative water column stability in reservoirs. The experimental data of de Lima et al. (2021) shown that FPV led to lower upper layer water temperature. Château et al. (2019) indicated that water temperature could be significantly reduced with a 40% FPV coverage ratio. Yang et al. (2021) developed a numerical model to predict the temperature of FPV panels, air

temperature, and water temperature below FPV panels, and compared it with measured data. Interestingly, the results of this study showed that water temperature under FPV panels increased. Most studies have only described the changes in water temperature caused by FPV, while the internal mechanism has not been fully revealed. Given these conflicting findings, currently, the impact of FPV on water temperature remains unclear. Theoretical research in this area is lacking, and there is also a lack of detailed assessment of existing experimental and theoretical results. Due to the complexity of the behaviour of waterbody thermal structure, it is necessary to reveal the influence mechanism of FPV on water temperature through long-term measured data. Considering the importance of FPV for the development and utilization of energy-water resources and global climate change, this is an urgent need. Therefore, this paper carries out field monitoring and numerical simulation based on a large-scale FPV power station. The innovation of this paper lies in monitoring and analyzing three-dimensional water temperature and meteorological parameters of large-scale FPV power stations for the first time. A numerical simulation model has been established that fully considers various heat transfer processes, helping to reveal the mechanisms of FPV's impact on the water energy balance. It also provides a feasible solution for simulating water temperature and assessing the impact of FPV construction on the aquatic environment in the future. The research objectives comprise: (1) Using empirical data, clarify the influence of FPV on water temperature and local microclimate; (2) Explore the relationship between the effect of FPV on water temperature and meteorological parameters; (3) Clarify the water energy balance under FPV shielding and establish the corresponding numerical simulation model; (4) Reveal the influence mechanism of FPV on water temperature and the changes of various heat budget terms under FPV shielding.

2 Experimental Design

2.1 Field Experiment

This work was carried out in Huainan City, Anhui Province, China (Fig. 1a). Huainan City is in the transition zone between the warm temperate zone and the subtropical zone, with an annual average temperature of 16.6 °C. The annual precipitation is 893.4 mm, and the seasonal precipitation is unevenly distributed. The annual sunshine duration is 1922.2 hours, and the annual sunshine percentage is 43%. The field monitoring carried out is based on the 150 MW FPV power station, which covers an area of approximately 4.5 km^2, and consists of several different photovoltaic module clusters (Fig. 1b). The FPV power station was officially connected to the grid in December 2017, with an annual power generation of about 1.5×10^8 kWh. In this paper, one of the coal mining subsidence areas where the FPV power station is located is selected as the research area, whose water surface coverage ratio is about 8.12%. Monitoring is based on controlled trials. Sites below the FPV panels and away from FPV arrays are set to respectively represent “below the FPV panels” and “open waters” conditions. The distance between the two monitoring sites is about 200 m.

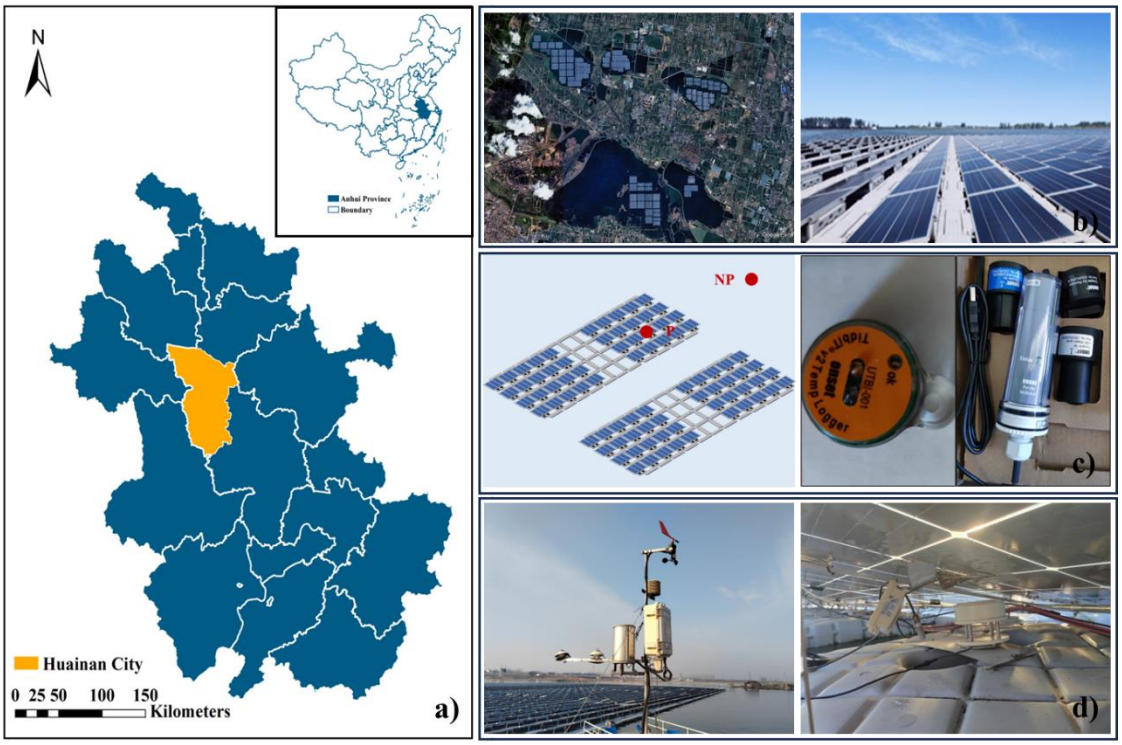

Fig. 1 Study area and monitoring designs

(a)-b) Study area; c) Water temperature monitoring (NP: open waters, P: below the FPV panels); d) meteorological parameters monitoring).

2.2 Measurements and Sensors

Water temperature sensors (HOBO MX2201) were operated from 11 Oct 2022 to 9 Mar 2023 at depths of 0.5, 2, 3, and 4 m below the water surface and installed below and away from the FPV arrays to respectively represent “below the FPV panels” and “open waters” conditions (Fig. 1c). Water temperature data was recorded at hourly intervals.

As meteorological conditions affect water temperature and energy balance, a solar radiation sensor (Kipp&Zonen CMP10), wind speed and direction sensor (MetOne 010C/020C), ambient temperature and humidity sensor (Vaisala HMP155A) were synchronously operated to monitor the local meteorological parameters from over the same period. In addition, the meteorological parameters below the FPV panels and the temperature of the FPV module back sheet (PT100) were monitored synchronously (Fig. 1d). These data were collected every minute.

3 Energy Balance Numerical Modelling

The change in water temperature is affected by the energy balance. Shortwave and longwave radiation, along with sensible and latent heat fluxes, jointly drive changes in water temperature. When analysing the impact of energy balance on water temperature, the following methods are used to relate the heat fluxes to the change in water temperature. To calculate the heat fluxes of a waterbody, we need to consider the water column per unit area from the surface to the bottom. During the period $\Delta t_{t_1-t_2}$, the heat corresponding to the temperature change of the water column should be equal to the sum of the four heat fluxes mentioned above. It is important to note that transverse convection heat transfer and bottom heat transfer are ignored in this calculation method.

3.1 The Energy Balance of Open Waters

The energy balance of open waters in the period $\Delta t_{t_1-t_2}$ can be described as Equation (1):

$$\frac{\sum_t C_w \rho_w h_i^w \left(T_{i,t_1}^w - T_{i,t_2}^w\right)}{\Delta t_{t_1-t_2}} = Q_{t_1-t_2}^{SW} + Q_{t_1-t_2}^{LW} + Q_{t_1-t_2}^{L} + Q_{t_1-t_2}^{S} \quad (1)$$

where C_w is the specific heat capacity of water (4185.8 J/kg/°C); ρ_w is the density of water (1000 kg/m^3); h_i^w is the thickness of water column at layer i (m); T_{i,t_1}^w is the T_w at time t_1 and layer i (°C); T_{i,t_2}^w is the T_w at time t_2 and layer i (°C); $\Delta t_{t_1-t_2}$ is the interval from t_1 to t_2 (s); $Q_{t_1-t_2}^{SW}$ is the average shortwave radiation in the period of $\Delta t_{t_1-t_2}$ (W/m^2); $Q_{t_1-t_2}^{LW}$ is the average longwave radiation in the period of $\Delta t_{t_1-t_2}$ (W/m^2); $Q_{t_1-t_2}^{L}$ is the average latent heat flux in the period of $\Delta t_{t_1-t_2}$ (W/m^2); $Q_{t_1-t_2}^{S}$ is the average sensible heat flux in the period of $\Delta t_{t_1-t_2}$ (W/m^2).

The shortwave radiation is calculated according to meteorological station data and water surface albedo as follows (Mady et al., 2021):

$$Q^{SW} = (1-\alpha_w) Q^{SR} \quad (2)$$

where α_w is the water surface albedo (0.05, referring to Cazzaniga and Rosa-Clot, (2021)); Q^{SR} is the solar radiation (W/m^2).

The Swinbank formula is used to calculate the net longwave radiation (Mady et al., 2021).

$$Q^{LW} = \sigma\left[\varepsilon_a (T^a + 273.15)^4 - \varepsilon_w (T^{w-s} + 273.15)^4\right] \quad (3)$$

$$\varepsilon_a = 0.711 + 0.56\left(\frac{T^{dew}}{100}\right) + 0.73\left(\frac{T^{dew}}{100}\right)^2 \quad (4)$$

where σ is Stephan-Boltzmann constant (5.67 × 10^{-8} W/m^2/K^4); ε_a is the emissivity of atmospheric; ε_w is the emissivity of water (0.96, referring to Yang et al. (2021)); T^a is the air temperature (°C); T^{w-s} is the water surface temperature (°C); T^{dew} is the dewpoint temperature (°C).

Latent heat flux is calculated as (Mady et al., 2021):

$$Q^L = \frac{D_a L}{\delta}(C_s - C_a) \quad (5)$$

where D_a is the vapor diffusion coefficient in air (2.5×10^{-5} m^2/s); L is the latent heat of vaporization (2,453,000 J/kg); δ is the viscous boundary layer thickness (0.005 m, referring to Mady et al. (2021)); C_s is the saturated vapor concentration at water temperature T^{w-s} (kg/m^3); C_a is the actual vapor concentration at air temperature T^a (kg/m^3).

Sensible heat flux is calculated as (Mady et al., 2021):

$$Q^S = \frac{K_a}{\delta}(T^a - T^{w-s}) \quad (6)$$

where K_a is the air thermal conductivity (0.024 W/m/K).

3.2 The Energy Balance of FPV Covered Water Area

The energy balance in the FPV covered water area is affected by the presence of the FPV. A unit of the FPV is defined as the water area where a single FPV module and its surrounding high-density polyethylene (HDPE) floats are located. There are three states of water surface in each unit:

the exposed water surface below the FPV panel (S^{W_PV}), the water surface under HDPE floats (below the FPV panels/at working channel) (S^{HDPE_PV} / S^{HDPE}), and the exposed water at the working channel (S^{W}) (as shown in Fig. 2). The energy balance of the unit is influenced by the energy transfer of the FPV modules, HDPE floats, and the atmosphere. This can be expressed as:

$$\frac{\sum_{i} C_w \rho_w h_i^w \left(T_{i,t_1}^{w\_pv} - T_{i,t_2}^{w\_pv}\right)}{\Delta t_{t_1\_t_2}} = Q_{t_1\_t_2}^{PV} + Q_{t_1\_t_2}^{HDPE} + Q_{t_1\_t_2}^{ATM} \tag{7}$$

where $T_{i,t_1}^{w\_pv}$ is the T_w below the FPV panels at time t_1 and layer i (°C); $T_{i,t_2}^{w\_pv}$ is the T_w below the FPV panels at time t_2 and layer i (°C); $Q_{t_1\_t_2}^{PV}$ is the average energy transfer between the FPV panels and water in the period of $\Delta t_{t_1\_t_2}$ (W/m^2); $Q_{t_1\_t_2}^{HDPE}$ is the average energy transfer between HDPE floating bodies and water in the period of $\Delta t_{t_1\_t_2}$ (W/m^2); $Q_{t_1\_t_2}^{ATM}$ is the average energy transfer between atmosphere and water in the period of $\Delta t_{t_1\_t_2}$ (W/m^2).

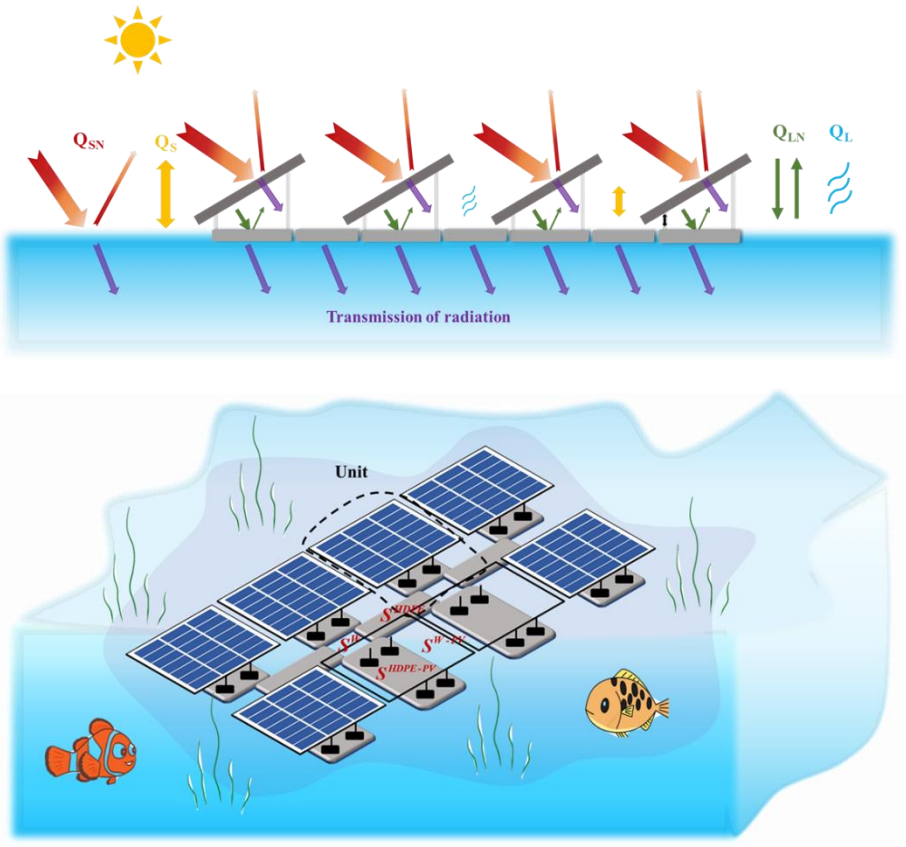

Fig. 2 Schematic diagram of energy balance in FPV construction water area.

The energy transfer between the FPV panels and the exposed water below is mainly through heat radiation.

$$Q^{PV} = \frac{Q^{LN\_PV} \times S^{W\_PV}}{S^{W\_PV} + S^{W} + S^{HDPE\_PV} + S^{HDPE}} \tag{8}$$

$$Q^{LN\_PV} = \sigma\left[\varepsilon_{pv}(T^{pv} + 273.15)^4 - \varepsilon_{w}(T^{w\_s\_pv} + 273.15)^4\right] \tag{9}$$

where Q^{LN_PV} is the longwave radiation between the FPV panels and water (W/m^2); T^{pv} is the temperature of FPV module back sheet (°C); $T^{w\_s\_pv}$ is the water surface temperature below the FPV panels (°C); ε_{pv} is the emissivity of photovoltaic panels (0.91, referring to Yang et al. (2021)).

Q^{HDPE} is the energy flux from the HDPE floats to the water surface, accounting for the energy stored in the floats that does not transfer to the atmosphere in the form of radiation or convection (Mady et al., 2021).

$$Q^{HDPE} = \frac{(Q^{SW\_PV\_HDPE} + Q^{LW\_PV\_HDPE} + Q^{S\_PV\_HDPE}) \times S^{PV\_HDPE} + (Q^{SW\_HDPE} + Q^{LW\_HDPE} + Q^{S\_HDPE}) \times S^{HDPE}}{S^{PV\_W} + S^{W} + S^{PV\_HDPE} + S^{HDPE}} \tag{10}$$

$$Q^{SW\_PV\_HDPE} = \gamma_1 Q^{SR} \tag{11}$$

$$Q^{LW\_PV\_HDPE} = \sigma\left[\varepsilon_{pv}(T^{pv} + 273.15)^4 - \varepsilon_{HDPE}(T^{pv\_HDPE} + 273.15)^4\right] \tag{12}$$

$$Q^{S\_PV\_HDPE} = h^{*}(T^{a\_pv} - T^{pv\_HDPE}) \tag{13}$$

$$Q^{SW\_HDPE} = (1 - \alpha_{HDPE})Q^{SR} \tag{14}$$

$$Q^{LW\_HDPE} = \sigma\left[\varepsilon_{a}(T^{a} + 273.15)^4 - \varepsilon_{HDPE}(T^{HDPE} + 273.15)^4\right] \tag{15}$$

$$Q^{S\_HDPE} = h^{*}(T^{a} - T^{HDPE}) \tag{16}$$

where $Q^{SW\_PV\_HDPE}$ is the shortwave radiation received by the floats below the FPV panels (W/m^2); γ_1 is the ratio of the amount of shortwave radiation received by the floats/water surface below the FPV panels to the amount of solar radiation (assumed herein to be 0.20, referring to Bax et al. (2023) and Ilgen et al. (2023)); $Q^{LW\_PV\_HDPE}$ is the longwave radiation received by the floats below the FPV panels (W/m^2); ε_{HDPE} is the emissivity of the floats (0.96, referring to Mady et al. (2021)); T^{pv_HDPE}

is the temperature of the floats below the FPV panels (°C); $Q^{S\_PV\_HDPE}$ is the sensible heat flux of the floats below the FPV panels (W/m^2); h* is the heat transfer coefficient (5 W/m^2/K is used as the natural convection heat transfer coefficient of air); T^{a_pv} is the air temperature below the FPV panels (°C); Q^{SW_HDPE} is the shortwave radiation received by the floats at the working channel (W/m^2); α_{HDPE} is the albedo of the floats (for the grey floats used here, the median value of white and black covers in Mady et al. (2021) is taken); Q^{LW_HDPE} is the longwave radiation received by the floats at the working channel (W/m^2); T^{HDPE} is the temperature of the floats at the working channel (°C); Q^{S_HDPE} is the sensible heat flux of the floats at the working channel (W/m^2).

The energy transfer between the atmosphere and the open water is calculated as:

$$Q^{ATM} = \frac{(Q^{SW\_PV\_W} + Q^{L\_PV\_W} + Q^{S\_PV\_W}) \times S^{PV\_W} + (Q^{SW} + Q^{LW} + Q^{L} + Q^{S}) \times S^{W}}{S^{PV\_W} + S^{W} + S^{PV\_HDPE} + S^{HDPE}} \tag{17}$$

$$Q^{SW\_PV\_W} = \gamma_1 Q^{SR} \tag{18}$$

$$Q^{L\_PV\_W} = \frac{D_a L}{\delta^{pv}} (C_s^{pv} - C_a^{pv}) \tag{19}$$

$$Q^{S\_PV\_W} = \frac{K_a}{\delta^{pv}} (T^{a\_pv} - T^{w\_s\_pv}) \tag{20}$$

where $Q^{SW\_PV\_W}$ is the shortwave radiation received by the water surface below the FPV panels (W/m^2); $Q^{L\_PV\_W}$ is the latent heat flux for the water surface below the FPV panels (W/m^2); δ^{pv} is the viscous boundary layer thickness below the FPV panels (m) (herein, it is assumed that $\delta^{pv} = \delta$); C_s^{pv} is the saturated vapor concentration at water temperature $T^{w\_s\_pv}$ (kg/m^3); C_a^{pv} is the actual vapor concentration at air temperature T^{a_pv} (kg/m^3); $Q^{S\_PV\_W}$ is the sensible heat flux for the water surface below the FPV panels (W/m^2).

Pearson's correlation coefficient (r) and the mean bias error (MBE) are used to measure the correlation and bias between calculation and simulation results, and calculated as, respectively:

$$r = \frac{\sum_{i=1}^{n}(h_c^i - \overline{h_c})(h_m^i - \overline{h_m})}{\sqrt{\sum_{i=1}^{n}(h_c^i - \overline{h_c})^2}\sqrt{\sum_{i=1}^{n}(h_m^i - \overline{h_m})^2}} \quad (21)$$

$$MBE = \frac{1}{n} \times \sum_{i=1}^{n}(h_c^i - h_m^i) \quad (22)$$

where i is the current calculation time step and n is the total number of samples; h_c is the calculated net heat flux (W/m^2); h_m is the modeled net heat flux (W/m^2).

4 Results and Discussion

4.1 Daily Dynamics of Water Temperature

Plots of the hourly water temperature-time series are derived from the field monitoring data from the different monitoring sites. Preliminary analysis using independent sample Mann-Whitney U tests, time-lagged correlation analysis, and other statistical analyses is conducted to reveal the influence of FPV on water temperature.

Fig. 3 shows the time series of water temperature at depths of 0.5, 2, 3 and 4 meters during the monitoring period. The water temperature at both the FPV and open water sites exhibits diurnal variations that decrease with depth. Compared to the open water, the peak water temperature below the FPV panels is significantly reduced. The diurnal fluctuation of water temperature is weakened, the FPV having a cooling effect during the daytime and an insulation effect at night. Specifically, during the daytime (7 a.m. to 7 p.m.), the water temperature below the FPV panels at a depth of 0.5 meters is typically 0.16°C cooler than that in open waters, with a maximum difference of 2.3°C. At night (7 p.m. to 7 a.m.), the water temperature below the FPV panels at 0.5 meters depth may be up to 0.98°C warmer than that in open waters, with an average increase of 0.01°C. According to the Mann-Whitney U test, the water temperature series at the two sites have no significant statistical difference ($p>0.05$).

This is likely due to the study period, including winter, during which the water temperature difference between the two sites is very small. As a result, the data series' overall distribution difference is insignificant. It also shows that the impact of FPV on water temperature is affected by meteorological conditions. A lag correlation analysis conducted by MATLAB reveals that the water temperature-time series of the FPV and open water sites have the strongest correlation when there is a two-hour time difference between them, with the change in water temperature below the FPV panels delayed compared to that of the open water site.

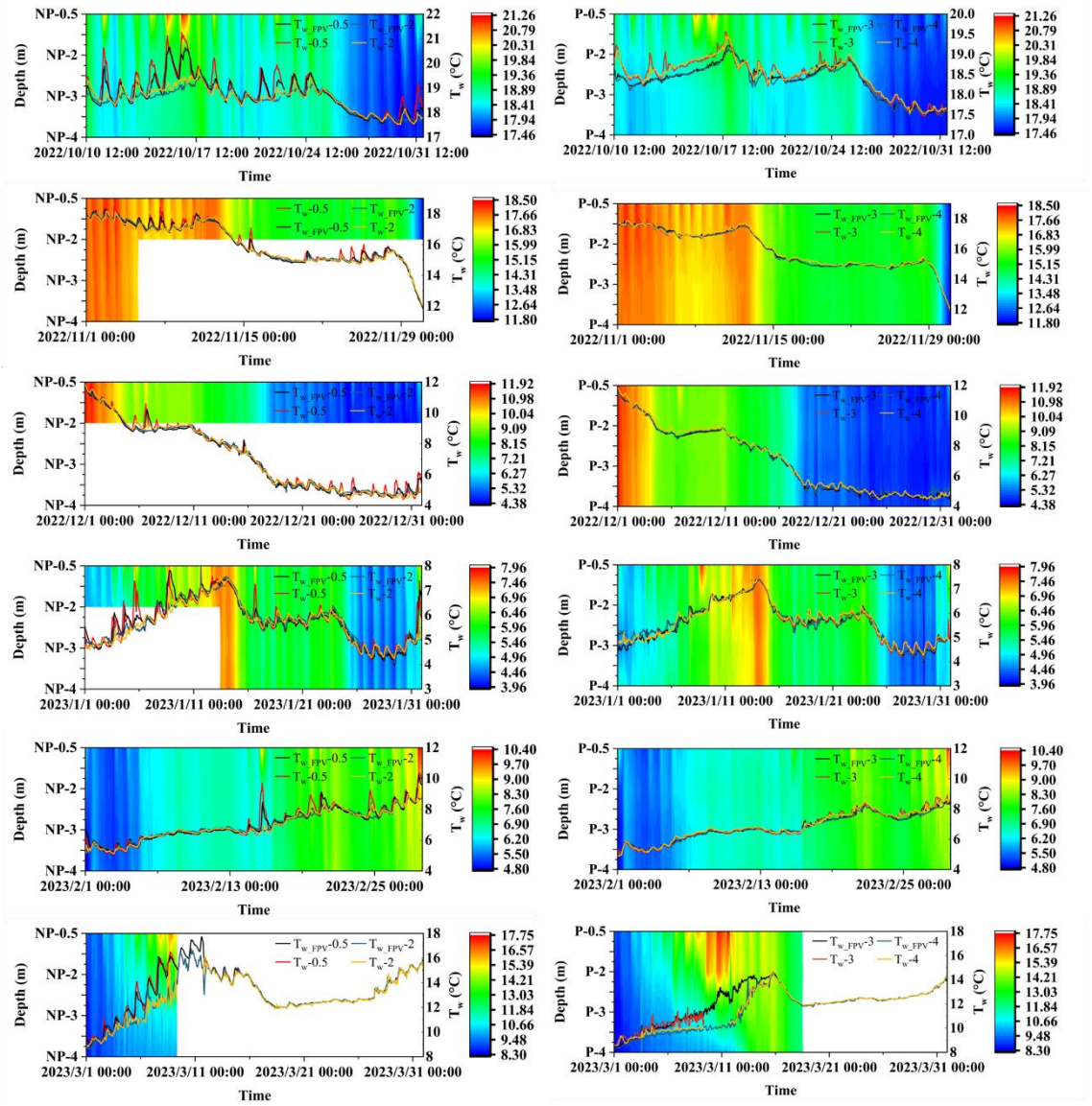

Fig. 3 Measurements of water temperature in the open waters (T_w) and below the FPV panels (T_{w_FPV}).

Fig. 3 also shows the vertical profiles of water temperature at the two monitoring sites. During the daytime, the surface water temperature below the FPV panels is noticeably cooler than that of open waters, presumably due to the decreased shortwave radiation. However, the bottom water temperature does not respond as much. At night, the water temperature difference at the bottom of the two sites is similar to that during the daytime. The surface water temperature difference between the FPV and open water sites is less than that at the bottom due to the thermal insulation effect of FPV. Thus, the temperature difference between the bottom and surface layers in the FPV covered area decreases during the daytime and increases at night. The variation in temperature and density below the FPV panels leads to decreased water column stability during the daytime and increased stability at night. These phenomena are observed in the transition zone between the warm temperate and subtropical climate zones, in a shallow lake during autumn and winter. It can be inferred that in a tropical climate or a deep-water reservoir with a constant bottom water temperature, the cooling effect of FPV will be more significant, leading to a greater reduction in water column stability.

4.2 Comparison of Meteorological Data

Water temperature is expected to be affected by changes in external environmental conditions. Therefore, we compare the meteorological conditions in the open water area and below the FPV panels to study the impact of FPV on the local microclimate. The results can help to understand the mechanism behind the influence of FPV on water temperature.

Fig. 4 shows the contrast in air temperature between open waters and below the FPV panels over the data collection period. The air temperature below the FPV panels is higher than that in the open water area during the daytime, and lower at night. The maximum air temperature difference between the two sites is 10.55°C. Moreover, the air temperature variation in the open water area lags

behind that below the FPV panels by approximately two hours. This observation implies that the heat sources at the two sites are different. Monitoring data shows that the temperature of the FPV module back sheet could reach 55.3°C during the daytime, and it therefore evidently a significant heat source. The difference between the FPV module back sheet temperature and the air temperature below the FPV panels reaches a maximum of 33.6°C, and these two temperatures series change simultaneously with each other. Moreover, the differences between the water temperature and both the air temperature below the FPV panels and the temperature of the FPV module back sheet are both positive during the daytime with maximum values of 17.2°C and 35.24°C, respectively, while at night they are both negative. From these data, we infer that the FPV panels are heated by solar radiation during the daytime, and then act as an additional source of heat for the surrounding atmosphere and water.

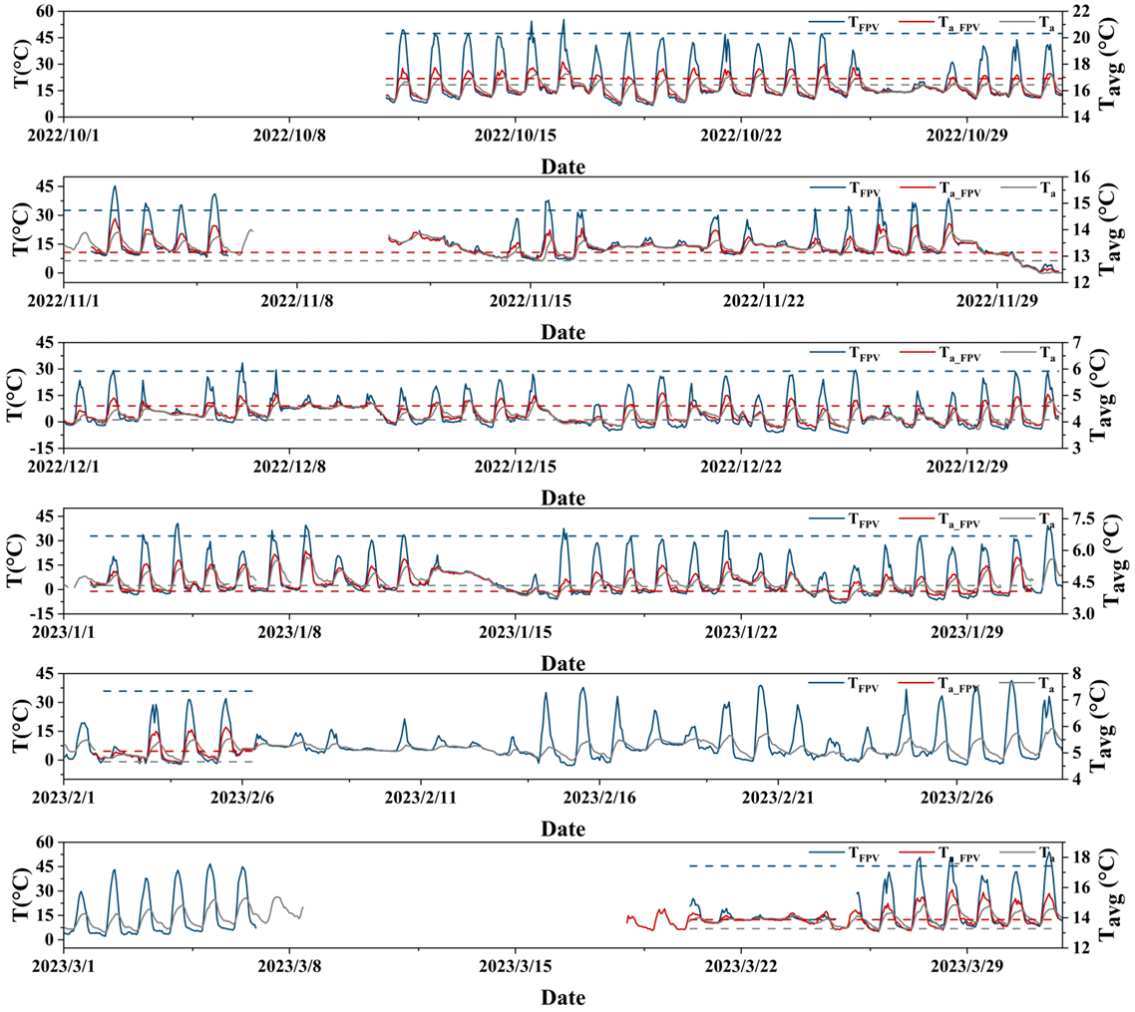

Fig. 4 Measurements of the temperature of FPV module back sheet (T_{FPV}), air temperature below the FPV panels (T_{a_FPV}) and in the open water area (T_a) (the dashed line represents the average temperature) in different months.

A consistent pattern of the relative humidity decreasing during the daytime and increasing at night is maintained at both the FPV and open water sites. Under the influence of FPV, the relative humidity further increases by 14.43% at night and decreases by 3.72% during the daytime (Fig. 5). The change in humidity level aids the process of evaporation during the daytime and inhibits it at night. In general, the effect of FPV on relative humidity is more prominent in inhibiting evaporation.

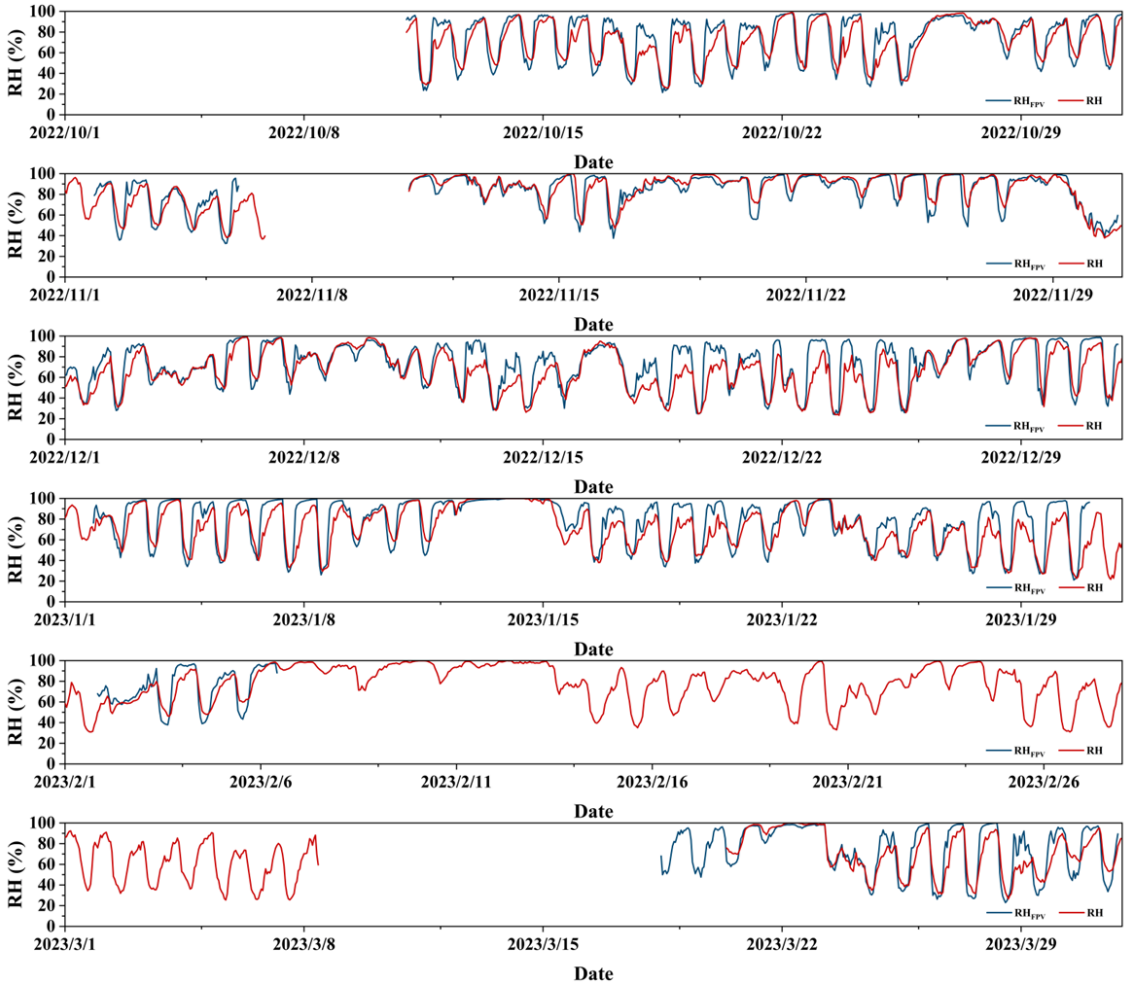

Fig. 5 Measurements of relative humidity below the FPV panels (RH_{FPV}) and in open waters (RH) in different months.

The shading of the FPV panels weakens the wind speed beneath them, but the extent of this effect is not clear from existing studies. To address this, we screen wind speed data greater than 2, 4, 6 and 8 m/s in turn, and calculate the ratio of wind speed above and below the FPV panels in each case (Fig. 6, some abnormal data are eliminated). The results show that the wind speed below the FPV panels is about 0.3 times that of the wind speed above FPV panels. The greatest weakening effect is observed when the wind comes from the southwest. The correlation between wind speed above and below the FPV panels shows unsignificant time correlation, possibly due to different effects of FPV on the wind in different directions. According to the Dalton evaporation formula, the effect on wind speed would significantly reduce the water evaporation rate, which is synergistic with the influence of relative humidity at night.

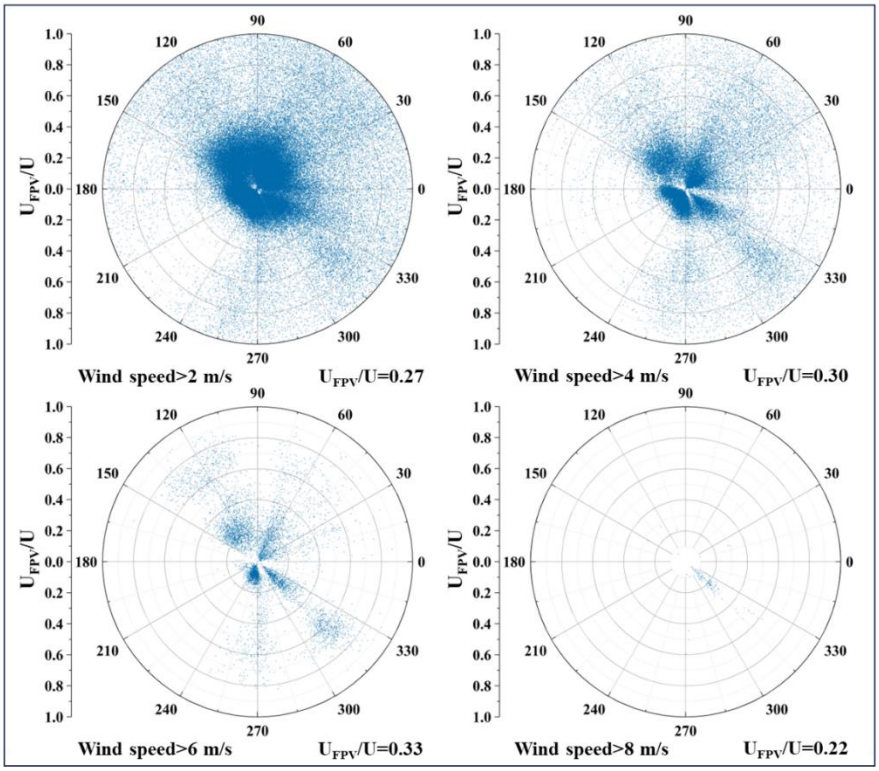

Fig. 6 The ratio of wind speed above (U) and below (U_{FPV}) the FPV panels.

The data indicate that the influence of FPV on water temperature varies with meteorological conditions. The correlation analysis results presented in Fig. 7 demonstrate a significant positive correlation between water temperature and the temperature of FPV module back sheet, air temperature, relative humidity, and solar radiation, and a negative correlation with wind speed. The difference of water temperature between the two sites is positively correlated with the temperature of FPV module back sheet, air temperature, and solar radiation, and negatively correlated with relative humidity. The amount of solar radiation that reaches the water below the FPV panels is considerably reduced. Although FPV panels emit longwave radiation as a new heat source, it is insufficient to compensate for the weakening of solar radiation. As a result, with the increase of solar radiation, the temperature difference between the FPV and open water sites increases. During rainy days, the effect of solar radiation is weakened or eliminated, and the insulation effect of FPV panels becomes more prominent, which may result in the water temperature below the FPV panels being higher than that in the open

water site. As wind speed increases, forced convection enhances water mobility, which may lead to a decrease in the heat budget difference between the FPV and open water sites, but the effect depends on the wind direction. The average relative humidity below the FPV panels increases and the latent heat loss decreases, which offsets the effects of solar radiation, air temperature and FPV module back sheet on water temperature, thus reducing the water temperature difference between the FPV and open water sites. It can be inferred that the cooling effect of FPV will be more significant in tropical, humid, low wind speed or southwest wind dominated areas. Thus, the influence of FPV on water temperature is affected by local climate conditions, which may explain the inconsistent conclusions in previously reported results from different climate zones.

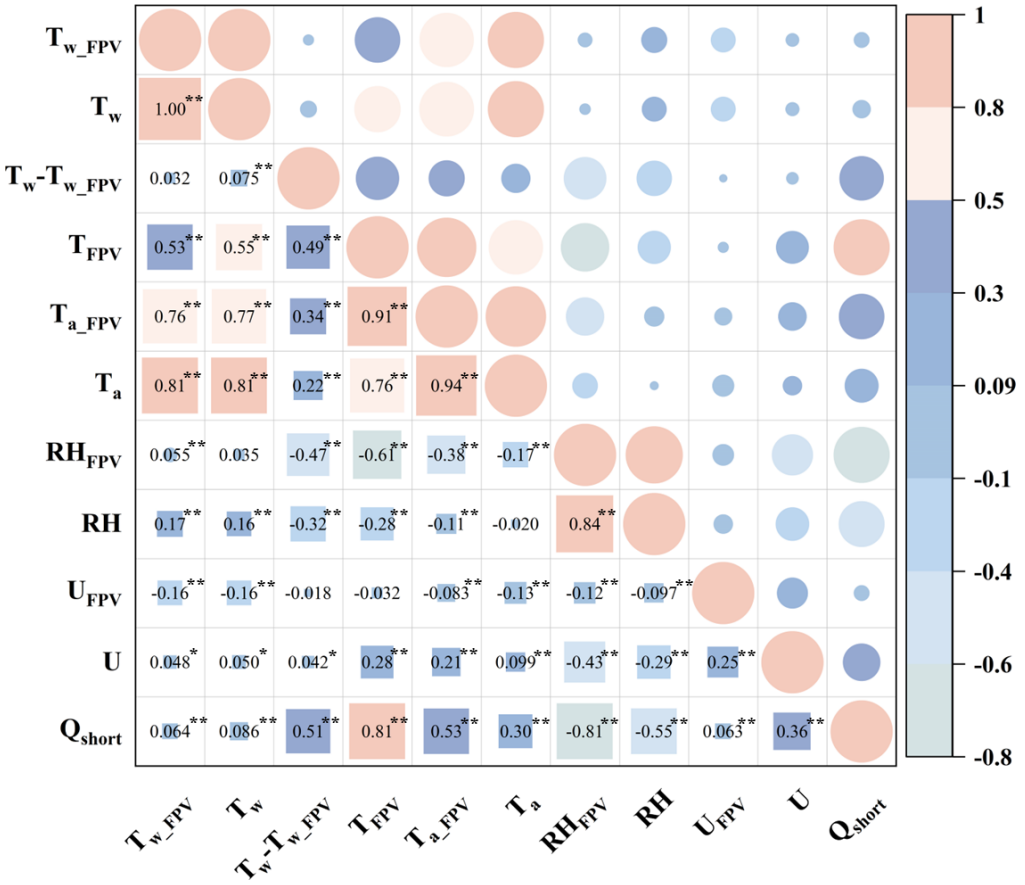

Fig. 7 The correlation between water temperature and meteorological parameters.

4.3 Modeling Energy Balance

The change of water temperature and vertical thermal structure is essentially a reflection of water energy balance, determined by solar radiation, longwave radiation, sensible heat flux and latent heat flux. In view of the rapid emergence of new FPV power stations under various environmental conditions, it is important to understand the energy balance in FPV-covered waters and establish a universal numerical model. When FPV panels are installed on water bodies, they act as a shield that limits the amount of solar radiation that penetrates the water surface. However, FPV panels also emits longwave radiation, which warms up the water. The microclimate conditions under FPV panels, including air temperature, wind speed and relative humidity are also changed, affecting the latent heat and sensible heat flux. Due to these factors, the heat stored in the water below the FPV panels decreases, and the variations in water temperature lags behind those in open waters.

By utilizing field monitoring data for solar radiation, air temperature, relative humidity, and wind speed, it is possible to simulate the net heat flux. Additionally, based on the measured water temperature and the specific heat capacity formula (the left side of Equation 1), the actual net heat flux stored or released by the water can be calculated. To ensure the smoothness of data, the actual net heat flux is processed using a sliding average filtering algorithm. Fig. 8 illustrates the daily net heat flux of open waters and the water below the FPV panels during the monitoring period. It indicates a good fit between modeled and actual net heat flux data, with the modeled results following the trends seen in the actual data. The simulation depends on various meteorological factors which have a lagging impact on the water temperature below the FPV panels. The correlation between the simulated and actual data is strongest when a time lag of one hour is applied, and the corresponding correlation coefficient is 0.82 ($p<0.05$). The mean bias error (MBE) is –6.77 W/m^2. Consistent with field observations, the water

below the FPV panels stores less heat than open waters during the daytime and loses less heat at night. The good general agreement between the modelled and actual net heat flux indicates that the results are reliable and that the numerical model can capture the energy balance characteristics of the FPV-covered water.

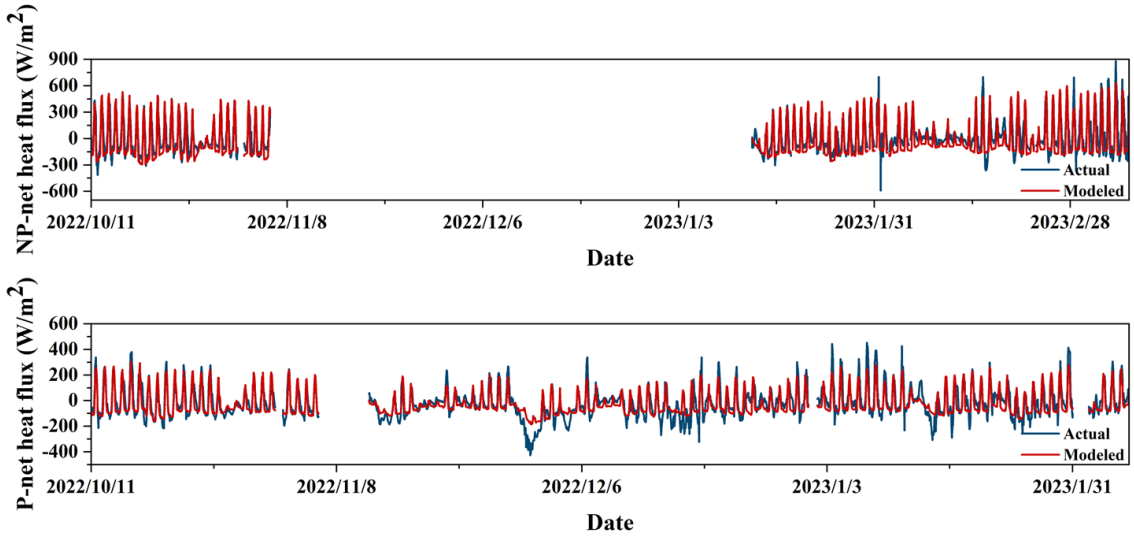

Fig. 8 Actual and modeled net heat flux in open waters and below the FPV panels.

Furthermore, we compare the value and composition of heat fluxes between the FPV and open water sites, to clarify the main factors affecting the water energy balance. Fig. 9 shows the heat fluxes below the FPV panels and in open waters. Compared with the open water site, shortwave radiation is significantly reduced under the FPV shielding. During the daytime, the longwave radiation changes from negative to positive and the main heat loss term switches from longwave radiation to latent heat flux. The sensible heat flux is dually affected by changes in water and air temperature below the FPV panels without significant changes, whereas the latent heat flux is significantly reduced. The detailed proportions of heat fluxes in the FPV and open water sites are shown in Table 1. For the water below the FPV panels, the main heat source in the daytime is shortwave radiation, followed by the longwave radiation, and finally the sensible heat flux. The main heat loss during the daytime changes from longwave radiation to latent heat flux.

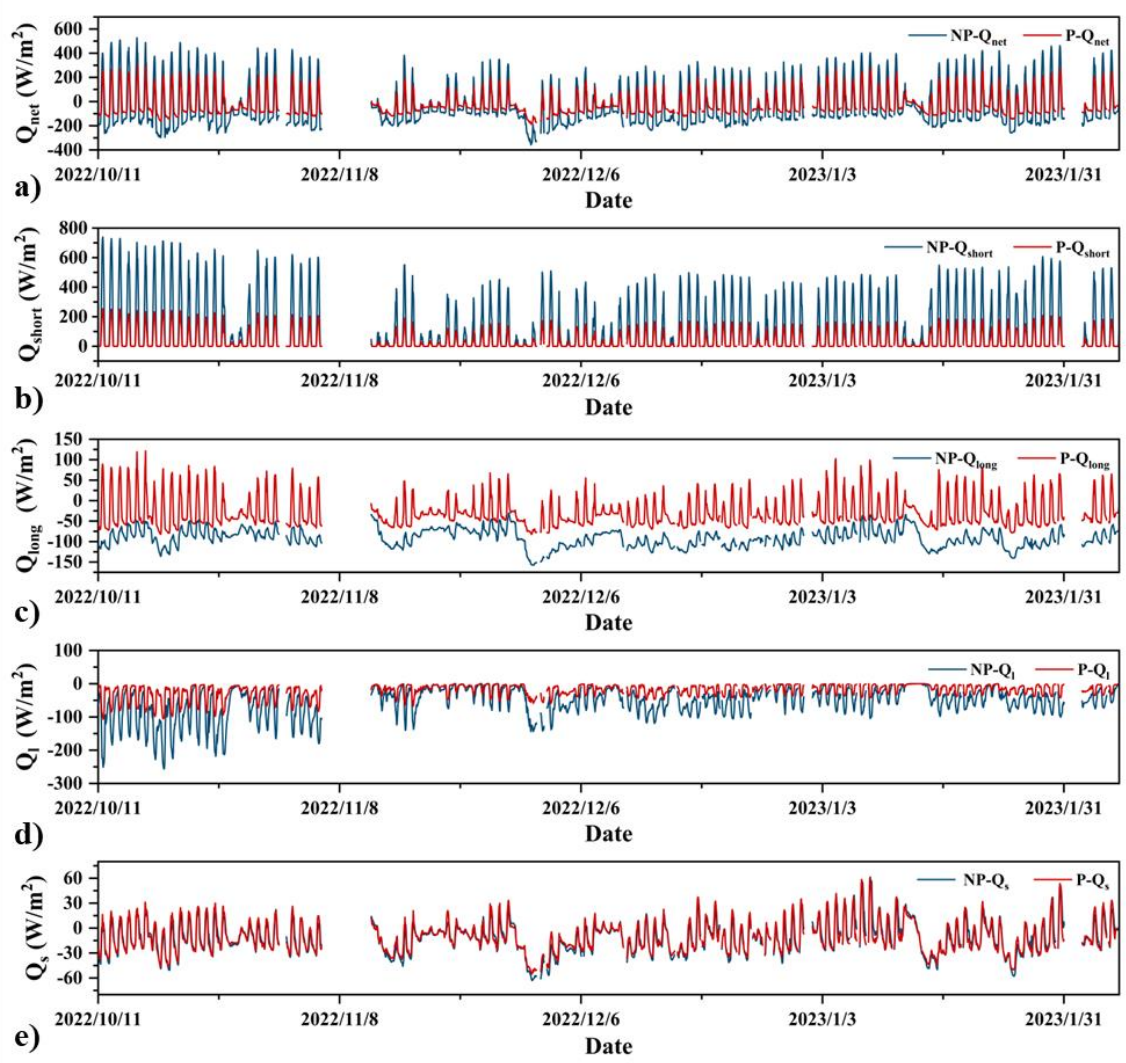

Fig.9 Heat fluxes below the FPV panels and in open waters (a) net heat flux; b) shortwave radiation; c) longwave radiation; d) latent heat flux; e) sensible heat flux).

Table 1 The proportion of various heat fluxes in open waters and below the FPV panels.

Site	Item	Q_{short} (%)	Q_{long} (%)	Q_l (%)	Q_s (%)
NP	Day-heat	97.66(+)	/	/	2.34(+)
	Day-loss	/	55.78(-)	37.67(-)	6.55(-)
	Night-loss	/	64.28(-)	25.08(-)	10.64(-)
P	Day-heat	83.39(+)	9.81(+)	/	6.80(+)
	Day-loss	/	36.31(-)	50.11(-)	13.58(-)
	Night-loss	/	65.12(-)	12.45(-)	22.43(-)

4.4 Suggestions and Limitations

Using the energy balance equations (7)-(20) presented above, the water temperature below the FPV panels can be calculated. This provides reference data for the aquatic environment impact

assessment before the deployment of FPV. When analyzing the impact of water surface heat exchange on water temperature, the following method is used to convert the water surface heat fluxes into equivalent temperature changes. On the premise of ignoring lateral convection and heat exchange, considering the epilimnion depth (h_D) (mixed layer), the heat required to cause temperature change in the water column (dT_{avg}) during a period (from time t_1 to t_2) should be equal to the sum of heat fluxes, as shown in Equation (23).

$$dT_{avg} = (t_2 - t_1)(Q^{SW}_{t_1 \_ t_2} + Q^{LW}_{t_1 \_ t_2} + Q^{L}_{t_1 \_ t_2} + Q^{S}_{t_1 \_ t_2}) / (h_D C_w \rho) \quad (23)$$

The water temperature at time t_2 (T_{t2}) should be equal to the sum of the water temperature at time t_1 (T_{t1}) and the change in water temperature (dT_{avg}), as shown in equation (24).

$$T_{t_2} = T_{t_1} + dT_{avg} \quad (24)$$

According to equations (23) and (24), the water temperature change processes occurring within the epilimnion can be estimated by the calculated heat fluxes. However, the epilimnion depth in the FPV construction water area may be affected by a combination of factors such as climates, seasons, and FPV panels. Despite the ubiquity of epilimnion depth, however, there is no objective or generic approach for defining the epilimnion, and a diverse number of approaches prevail in the literature (Wilson et al., 2020). According to the water temperature monitoring data, the water temperature at 0.5 meters fluctuates significantly during the daytime and is different from that at other depths. Therefore, using the water temperature at 0.5 meters as a reference, the h_D both in open waters and below the FPV panels are calculated. The h_D in open waters is about 1.43 meters during the daytime and 2.21 meters at night. The h_D below the FPV panels is about 1.34 meters during the daytime and 1.83 meters at night, which is about 0.1-0.4 meters lower than that in open waters. The vertical water temperature distribution data as shown in Fig.3 also indicates that the epilimnion depth below the FPV

panels is lower than that in open waters. Combined with the calculated heat fluxes in section 4.3, the net heat flux below the FPV panels is reduced by about 50% on average compared with that in open waters (Fig. 9a). Under the combined effect of FPV on net heat flux and h_D, the water temperature within epilimnion changes less than that in open waters. The influence of FPV on water temperature is less than that on net heat flux, showing a linear relationship with a coefficient less than 1. For similar shallow waters, when focusing on the water temperature changes caused by FPV on the intraday time scale, it is necessary to pay attention to the influence of changing meteorological conditions on the epilimnion depth. If FPV is constructed in a reservoir with obvious seasonal stratification, the changes in net heat flux and water temperature caused by FPV on seasonal time scales are more attractive. Attention should be paid to the obvious changes in the epilimnion depth due to seasonal changes in net heat flux. It can be inferred that FPV tends to reduce the epilimnion depth and increase the upper surface water level of the thermocline, especially in summer. With the expansion of the thermocline range, if the water intake flow and elevation are remained, it may further increase the risk of low-temperature water discharge, increase the frequency of anoxia in the water body, and affect the reproduction and growth of downstream fish.

In addition, the measured data shows that the influence range of FPV on water temperature is limited, and the overall water temperature distribution is not uniform. Especially when the coverage is low, FPV only affects the water temperature locally. The influence radius of FPV in this study is approximately 80 meters, which is around 20-25% of the length of each side of the FPV. According to equations (23) and (24), only the water temperature in open waters and below the FPV panels can be calculated respectively, without considering the lateral heat exchange in the transition region, and the result is difficult to reflect the real state of the water temperature distribution in the whole water area.

Therefore, it remains necessary to construct a three-dimensional numerical model to better understand the heat transfer processes and clarify the lateral range of influence of the FPV.

5 Conclusions

In this paper, the impact of FPV on the energy balance of its host waterbody is explored through empirical monitoring and numerical modeling. The results show that compared with open waters, the peak water temperature below the FPV panels decreases by up to 2.3°C, a difference which is especially significant on sunny days. Broadly speaking, FPV has a cooling effect during the daytime and a heat preservation effect at night. The diurnal fluctuation of water temperature is weakened. The cooling effect of FPV panels during the daytime is conducive to breaking down the thermal stratification and reducing the water column stability. Under the shading of FPV and its surrounding floats, the variation of water temperature below the FPV panel lags that in open waters by about two hours. The extent and direction of the impact on water temperature is affected by weather conditions and local environmental factors. The difference of water temperature between the FPV and open water sites is positively correlated with the temperature of the FPV module back sheet, air temperature, and solar radiation, and negatively correlated with relative humidity. It can be inferred that when the host waterbodies are in tropical, humid, low wind speed areas or deep-water reservoirs with a constant temperature at the bottom are considered, the impact of FPV on water temperature and water stability would be more significant.

Based on the measured data, the numerical model reflecting the changes of various heat fluxes effectively represents the energy balance characteristics of the host waterbody ($r=0.82$). Compared with the open water site, solar radiation reaching the water surface is significantly reduced by FPV shielding. During the daytime, the net longwave radiation changes from negative to positive, becoming

a new heat source for the water, and the main heat loss term switches from longwave radiation to latent heat flux. The latent heat flux decreases significantly under the combined effect of FPV on relative humidity, water temperature and air temperature, while the changes in sensible heat flux are not very noticeable. The energy balance and water temperature below the FPV panels are primarily controlled by the significant decrease in incoming shortwave radiation and outgoing longwave radiation and latent heat flux. Due to the balancing of cooling and insulation effects during the daytime and at night, FPV has an insignificant impact on water temperature. This indicates that the impact of FPV on water temperature is self-regulating throughout the day. Organisms that are vulnerable to daily temperature changes require more attention.

This paper reveals the impact of FPV on water temperature and energy balance through three-dimensional monitoring data and numerical modelling, which is expected to contribute to the improvement of the theoretical basis of this research field and the evaluation of the impact of FPV deployment. Further work is required to deepen and refine these findings, elucidate the long-term, cumulative effects of FPV on their host waterbodies' environment, and thus promote the sustainable development of FPV.

Declaration of Competing Interest

The authors declare that they have no known competing financial interests or personal relationships that could have appeared to influence the work reported in this paper.

Acknowledgments

This work was supported by the National Natural Science Foundation of China [grant number 52079087, 52279021] and the National Key Research and Development Program [grant number

2023YFC3209401]. We extend our sincere gratitude to the editor and the anonymous reviewers for their professional comments and corrections.

References

Assouline, S., Narkis, K., 2021, Reducing Evaporation From Water Reservoirs Using Floating Lattice Structures. WATER RESOUR RES 57. https://doi.org/10.1029/2021WR029670.

Bax, V., van de Lageweg, W.I., Hoosemans, R., van den Berg, B., 2023, Floating photovoltaic pilot project at the Oostvoornse lake: Assessment of the water quality effects of three different system designs. Energy reports 9, 1415-1425. https://doi.org/10.1016/j.egyr.2022.12.080.

Cazzaniga, R., Rosa-Clot, M., 2021, The booming of floating PV. SOL ENERGY 219, 3-10. https://doi.org/10.1016/j.solener.2020.09.057.

Château, P., Wunderlich, R.F., Wang, T., Lai, H., Chen, C., Chang, F., 2019, Mathematical modeling suggests high potential for the deployment of floating photovoltaic on fish ponds. SCI TOTAL ENVIRON 687, 654-666. https://doi.org/10.1016/j.scitotenv.2019.05.420.

de Lima, R.L.P., Paxinou, K., C. Boogaard, F., Akkerman, O., Lin, F., 2021, In-Situ Water Quality Observations under a Large-Scale Floating Solar Farm Using Sensors and Underwater Drones. SUSTAINABILITY-BASEL 13, 6421. https://doi.org/10.3390/su13116421.

Exley, G., Armstrong, A., Page, T., Jones, I.D., 2021, Floating photovoltaics could mitigate climate change impacts on water body temperature and stratification. SOL ENERGY 219, 24-33. https://doi.org/10.1016/j.solener.2021.01.076.

Gadzanku, S., Mirletz, H., Lee, N., Daw, J., Warren, A., 2021, Benefits and Critical Knowledge Gaps in Determining the Role of Floating Photovoltaics in the Energy-Water-Food Nexus. SUSTAINABILITY-BASEL 13, 4317. https://doi.org/10.3390/su13084317.

Gorjian, S., Sharon, H., Ebadi, H., Kant, K., Scavo, F.B., Tina, G.M., 2021, Recent technical advancements, economics and environmental impacts of floating photovoltaic solar energy conversion systems. J CLEAN PROD 278, 124285. https://doi.org/10.1016/j.jclepro.2020.124285.

Hooper, T., Armstrong, A., Vlaswinkel, B., 2021, Environmental impacts and benefits of marine floating solar. SOL ENERGY 219, 11-14. https://doi.org/10.1016/j.solener.2020.10.010.

Hosenuzzaman, M., Rahim, N.A., Selvaraj, J., Hasanuzzaman, M., Malek, A.B.M.A., Nahar, A., 2015, Global prospects, progress, policies, and environmental impact of solar photovoltaic power generation. Renewable and Sustainable Energy Reviews 41, 284-297. http://dx.doi.org/10.1016/j.rser.2014.08.046.

Ilgen, K., Schindler, D., Wieland, S., Lange, J., 2023, The impact of floating photovoltaic power plants on lake water temperature and stratification. SCI REP-UK 13. https://doi.org/10.1038/s41598-023-34751-2.

Ji, Q., Li, K., Wang, Y., Feng, J., Li, R., Liang, R., 2022, Effect of floating photovoltaic system on water temperature of deep reservoir and assessment of its potential benefits, a case on Xiangjiaba Reservoir with hydropower station. RENEW ENERG 195, 946-956. https://doi.org/10.1016/j.renene.2022.06.096.

Lehmann, P., Aminzadeh, M., Or, D., 2019, Evaporation Suppression From Water Bodies Using Floating Covers: Laboratory Studies of Cover Type, Wind, and Radiation Effects. WATER RESOUR RES 55, 4839-4853. https://doi.org/10.1029/2018WR024489.

Mady, B., Lehmann, P., Or, D., 2021, Evaporation Suppression From Small Reservoirs Using Floating Covers—Field Study and Modeling. WATER RESOUR RES 57. https://doi.org/10.1029/2020WR028753.

Manoj Kumar, N., Chakraborty, S., Kumar Yadav, S., Singh, J., Chopra, S.S., 2022, Advancing simulation tools specific to floating solar photovoltaic systems – Comparative analysis of field-measured and simulated energy performance. Sustainable Energy Technologies and Assessments 52, 102168. https://doi.org/10.1016/j.seta.2022.102168.

McKuin, B., Zumkehr, A., Ta, J., Bales, R., Viers, J.H., Pathak, T., Campbell, J.E., 2021, Energy and water co-benefits from covering canals with solar panels. Nature Sustainability 4, 609-617. https://doi.org/10.1038/s41893-021-00693-8.

Oliveira-Pinto, S., Stokkermans, J., 2020, Assessment of the potential of different floating solar technologies – Overview and analysis of different case studies. ENERG CONVERS MANAGE 211, 112747. https://doi.org/10.1016/j.enconman.2020.112747.

Rezazadeh, A., Akbarzadeh, P., Aminzadeh, M., 2020, The effect of floating balls density on evaporation suppression of water reservoirs in the presence of surface flows. J HYDROL 591, 125323. https://doi.org/10.1016/j.jhydrol.2020.125323.

Sahu, A., Yadav, N., Sudhakar, K., 2016, Floating photovoltaic power plant: A review. Renewable and Sustainable Energy Reviews 66, 815-824. http://dx.doi.org/10.1016/j.rser.2016.08.051.

Shalaby, M.M., Nassar, I.N., Abdallah, A.M., 2021a, Effect of continuous and modular floating covers on evaporation losses and microalgal growth. Journal of King Saud University - Engineering Sciences. https://doi.org/10.1016/j.jksues.2021.08.007.

Shalaby, M.M., Nassar, I.N., Abdallah, A.M., 2021b, Evaporation suppression from open water surface using various floating covers with consideration of water ecology. Journal of hydrology (Amsterdam) 598, 126482. https://doi.org/10.1016/j.jhydrol.2021.126482.

Solomin, E., Sirotkin, E., Cuce, E., Selvanathan, S.P., Kumarasamy, S., 2021, Hybrid Floating Solar Plant Designs: A Review. ENERGIES 14, 2751. https://doi.org/10.3390/en14102751.

Spencer, R.S., Macknick, J., Aznar, A., Warren, A., Reese, M.O., 2019, Floating Photovoltaic Systems: Assessing the Technical Potential of Photovoltaic Systems on Man-Made Water Bodies in the Continental United States. ENVIRON SCI TECHNOL 53, 1680-1689. https://doi.org/10.1021/acs.est.8b04735.

Trapani, K., Redón Santafé, M., 2015, A review of floating photovoltaic installations: 2007–2013. Progress in Photovoltaics: Research and Applications 23, 524-532. https://doi.org/10.1002/pip.2466.

Wilson, H.L., Ayala, A.I., Jones, I.D., Rolston, A., Pierson, D., de Eyto, E., Grossart, H., Perga, M., Woolway, R.I., Jennings, E., 2020, Variability in epilimnion depth estimations in lakes. HYDROL EARTH SYST SC 24, 5559-5577. https://doi.org/10.5194/hess-24-5559-2020.

Yang, K., Yu, Z., Luo, Y., Zhou, X., Shang, C., 2019, Spatial-Temporal Variation of Lake Surface Water Temperature and Its Driving Factors in Yunnan-Guizhou Plateau. WATER RESOUR RES 55, 4688-4703. https://doi.org/10.1029/2019WR025316.

Yang, P., Chua, L.H.C., Irvine, K.N., Imberger, J., 2021, Radiation and energy budget dynamics associated with a floating photovoltaic system. WATER RES 206, 117745. https://doi.org/10.1016/j.watres.2021.117745.

Zhou, Y., Chang, F., Chang, L., Lee, W., Huang, A., Xu, C., Guo, S., 2020, An advanced complementary scheme of floating photovoltaic and hydropower generation flourishing water-food-energy nexus synergies. APPL ENERG 275, 115389. https://doi.org/10.1016/j.apenergy.2020.115389.